Fusion Engineering and Design 104 (2016) 21–27

Contents lists available at ScienceDirect

Fusion Engineering and Design

journal homepage: www.elsevier.com/locate/fusengdes

Effect of tantalum content on microstructure and tensile properties of CLAM steel

Xiangwei Zhai [a,b], Shaojun Liu [a,*], Yanyun Zhao [a]

[a] Key Laboratory of Neutronics and Radiation Safety, Institute of Nuclear Energy Safety Technology, Chinese Academy of Sciences, Hefei, Anhui 230031, China
[b] University of Science and Technology of China, Hefei, Anhui 230027, China

HIGHLIGHTS

- With the increase of Ta content, the grain size decreased firstly, and then leveled off when Ta content was higher than 0.15 wt%.
- The content of Ta-riched MX particles increased with Ta content increasing, and the Cr-riched $M_{23}C_6$ carbides reversed.
- CLAM steel with Ta content of 0.027 wt% had the highest strength, but the difference in strength of the four ingots was little.

ARTICLE INFO

Article history:
Received 8 May 2015
Received in revised form 4 January 2016
Accepted 13 January 2016
Available online 5 February 2016

Keywords:
CLAM steel
Ta content
Ta-riched MX particle
Tensile properties

ABSTRACT

Four ingots of China Low Activation Martensitic (CLAM) steel with different Tantalum (Ta) contents of 0.027 wt%, 0.078 wt%, 0.15 wt% and 0.18 wt%, respectively, were produced by vacuum induction furnace. Microstructure observation and tensile tests were performed to make clear the effect of Ta content on the microstructure and properties of CLAM steel. Experimental results showed that the content of Ta-riched MX particles increased with Ta content increasing from 0.027 wt% to 0.18 wt%, and the Cr-riched $M_{23}C_6$ carbides reversed. Meanwhile, the grain size became finer with the increase of Ta content. However, the effect of Ta content on grain size refinement weakened when Ta content was higher than 0.15 wt% in this study. Both the grain size and precipitates could affect the tensile properties of the four ingots. The precipitation strengthening of Cr-riched $M_{23}C_6$ carbides was considered to be the main possible reason that CLAM steel with Ta content of 0.027 wt% had the highest strength. In general, there was little difference in strength of the four ingots with the change of Ta content.

© 2016 Elsevier B.V. All rights reserved.

1. Introduction

Reduced Activation Ferritic/Martensitic (RAFM) steels were considered as the reference structural materials for future fusion power reactors because of their relatively matured industrial infrastructure and relatively good neutron irradiation resistance [1]. During the past thirty years, a lot of research and development has been performed on RAFM steels, including ORNL 9Cr-2WVTa in USA, EUROFER in Europe, JLF-1 and F82H in Japan and CLAM steel in China [2–5].

Ta is an essential element for RAFM steels, which plays an important role in lowering DBTT through its effect on prior-austenitic grain size refinement [6] and improving the strength and toughness [7]. However, higher tantalum content can result in the formation of extremely coarse TaC carbide during the melting process, which is deleterious to the mechanical properties [8]. Furthermore, higher Ta content would also decrease the weldability [9]. Therefore, the effect of Ta content on the microstructure and the mechanical properties, especially the tensile properties, is one of the key issues for RAFMs to be finally applied to fusion DEMO reactor [10].

China Low Activation Martensitic (CLAM) steel with the nominal composition of 9Cr-1.5W-0.2V-0.15Ta-0.45Mn, has being developed in INEST (Institute of Nuclear Energy Safety Technology, Chinese Academy of Sciences) under wide collaboration with many institutes and universities during the recent ten years [5,11]. In China, the research and development activities on CLAM steel mainly cover composition design, melting and processing, impurity control [12], performance tests [13], microstructure analysis, fabrication techniques of test blanket module (TBM) [14–16], which consist of Hot Isostatic Pressing (HIP) joining and Electron Beam

* Corresponding author.
E-mail address: shaojun.liu@fds.org.cn (S. Liu).

http://dx.doi.org/10.1016/j.fusengdes.2016.01.016
0920-3796/© 2016 Elsevier B.V. All rights reserved.

Table 1
Chemical compositions (mass fracture %) of tested steels.

	C	Cr	W	V	Ta	Mn	Fe
1009A	0.11	8.56	1.66	0.18	0.027	0.44	Bal.
1009B	0.11	8.79	1.67	0.20	0.078	0.43	Bal.
1009C	0.10	9.13	1.60	0.21	0.15	0.47	Bal.
1009D	0.11	9.30	1.65	0.22	0.18	0.51	Bal.

Table 2
The estimation average grain sizes of HEATs 1009A-D.

	Average grain size (μm)	ASTM grain size number
1009A	24.2	7.4
1009B	11.1	9.7
1009C	8.3	10.5
1009D	8.2	10.6

Welding (EBW), fabrication of TBM mockups, tritium permeation barrier coating, compatibility with liquid eutectic PbLi [17], irradiation experiments and activation analysis, etc. [18]. In addition, it has been chosen as the structural material for the series of fusion-driven system designs developed by FDS team [19–31] and ITER TBM [32] in China. For the composition design of CLAM steel, maintaining Cr at 9 wt% provides the lowest ductile-brittle transition temperature (DBTT) before and after irradiation. The W content chosen as 1.5 wt% could decrease the possibility of Laves phase precipitation and effectively improve the strength at on-service temperature. The Ta content of 0.15 wt% is much higher than that of other RAFM steels to refine the grain size and improve creep resistance at elevated temperature. At the same time, the compositions optimization is also in progress. In this paper, the effect of Ta content varied from 0.027 wt% to 0.18 wt% on the microstructure and the tensile properties of CLAM steel were investigated. This work aims at further systematic understanding the effect of Ta content on precipitation behavior and mechanical properties of RAFM steels.

2. Experimental procedure

Four 25 kg ingots were prepared using vacuum induction furnace with Ta contents of 0.027 wt%, 0.078 wt%, 0.15 wt% and 0.18 wt%, respectively, and named as HEAT 1009A, HEAT 1009B, HEAT 1009C and HEAT 1009D, accordingly. The chemical compositions of the four ingots are listed in Table 1.

All HEATs were hot-forged at 1423 K and then rolled into 12 mm thick plates. The plates were quenched by air after holding at 1253 K for 30 min, followed by tempered at 1033 K for 90 min, and subsequently cooled by air.

The specimens for tensile tests were machined from the 12 mm plate material in parallel with the rolling direction. Round-bar tensile specimens with gauge of $\Phi 4 \times 20\,mm^2$ were tested on an MTS SHT5206-P testing machine at temperatures ranging from room temperature (RT) to 873 K, according to ISO 783:1989. The yield strength (YS) was measured by the 0.2% proof strength.

Microstructural investigations were performed by optical microscopy (OM), scanning electron microscopy (SEM), energy dispersive X-ray spectrum (EDS) and transmission electron microscope (TEM). The samples for metallographic observation were etched in an alcohol solution of picric acid and muriatic acid.

3. Results and discussion

3.1. Microstructure observation and analysis

Fig. 1 shows the metallographic images of the four HEATs. It could be found that all the four HEATs have the typical tempered martensitic structure. The estimated average grain sizes of HEATs 1009A-D by OM are shown in Table 2. The ASTM (American Society for Testing and Materials) grain size numbers are 7.4, 9.7, 10.5 and 10.6 for the four HEATs, respectively. For the four composition points, the grain becomes finer with the increase of Ta content

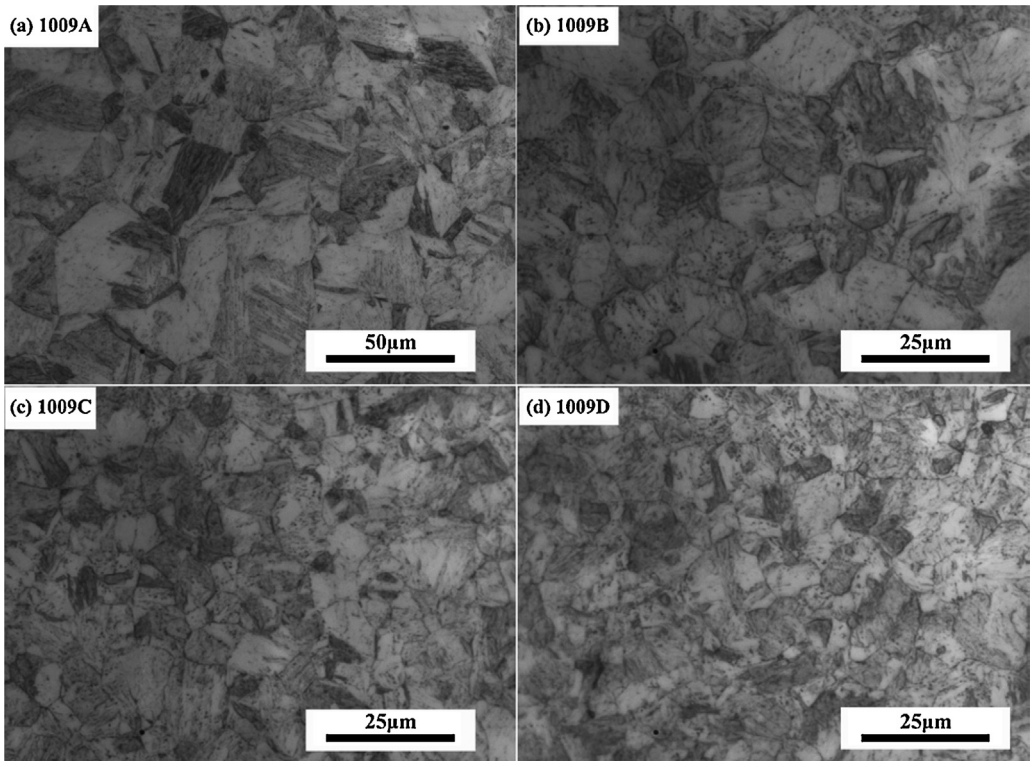

Fig. 1. Metallographic observation of HEATs 1009A-D.

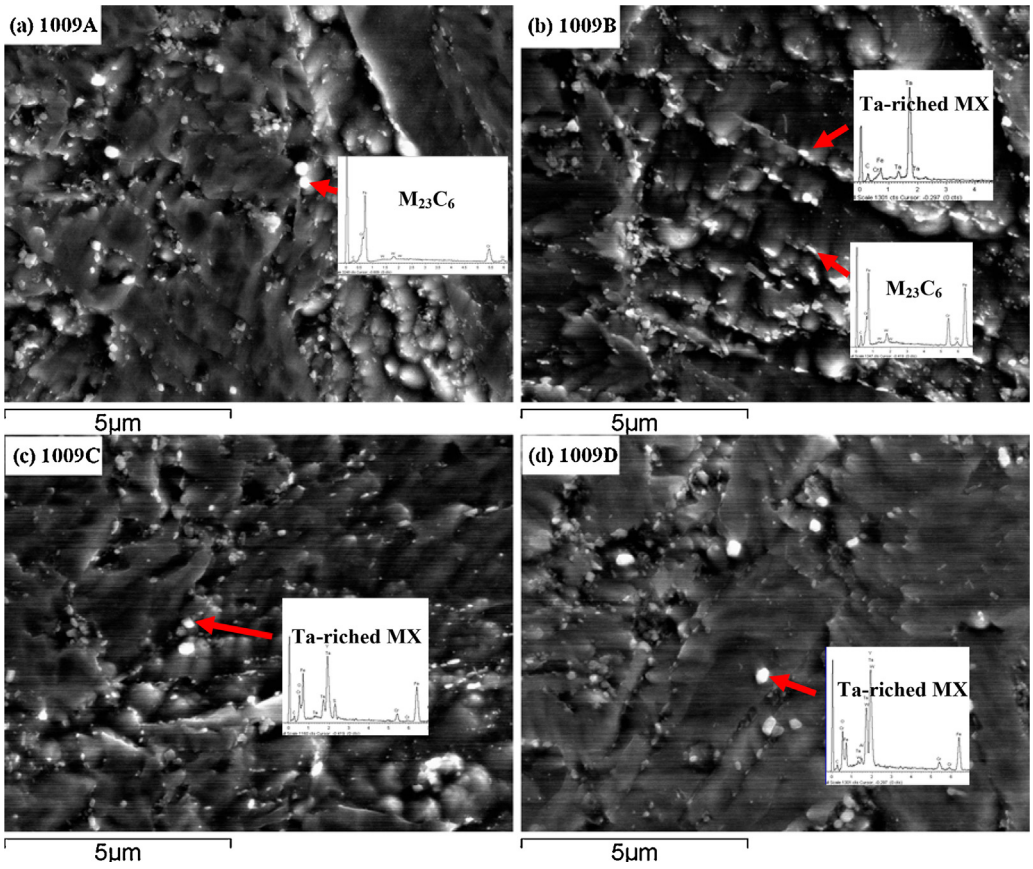

Fig. 2. SEM and EDS observation for the precipitates in HEATs 1009A-D.

ranging from 0.027 wt% to 0.15 wt%; and when Ta content exceeds 0.15 wt%, there is no obvious change of the ASTM grain size. It implies that the effect of Ta content on the grain size refinement is strong at first, then no longer apparent under the condition of the conventional heat treatment, as Ta content increases from 0.027 wt% to 0.18 wt%.

SEM and EDS images for the specimens of HEATs 1009A-D are shown in Fig. 2. Two kinds of precipitates with different morphologies, including $M_{23}C_6$ and MX, could be observed. Similar results for other RAFMs were reported as well [33]. The EDS analysis shows that most of the precipitates in HEAT 1009A are Cr-riched $M_{23}C_6$ carbides, and that the Ta-riched MX particles increase gradually in HEATs 1009B-D. SEM images also show the variation of precipitates with the change of Ta content. Cr-riched $M_{23}C_6$ carbides (~100–150 nm size) were distributed preferentially along grain and subgrain boundaries, while Ta-riched MX particles (~20–50 nm size) were located mainly in the matrix [34,35]. It could be observed that the content of Cr-riched $M_{23}C_6$ carbides in HEAT 1009B decreases compared with HEAT 1009A. When Ta content is less than or equal to 0.078 wt%, dispersed fine Ta-riched MX particles are observed significantly, and with the increase of Ta content (up to 0.15 wt%), the size of fine Ta-riched MX particles increases and some coarse Ta-riched MX particles could be found. When Ta content reaches 0.18 wt%, plenty of coarse Ta-riched MX particles with larger size are observed.

TEM images are shown in Fig. 3. According to the EDS results and the previous work [34], small globular particles were mainly Ta-riched MX particles. It could be seen that the amount and the size of Ta-riched MX precipitates increase with the increase of Ta content. Small globular precipitates are rarely found in the lath of HEAT 1009A. There are some globular precipitates in the lath of the HEAT 1009B with the size of about 10–30 nm. In HEATs 1009C and 1009D, some precipitates are in the lath or along the lath boundaries with greater size than that of the HEATs 1009A and 1009B.

As a strong carbide-forming element, Ta contributes to the formation of hard MC carbides, and can decrease the amount of $M_{23}C_6$ carbides [35]. It could be regarded as the factor of the reduction of Cr-riched $M_{23}C_6$ carbides from HEATs 1009A to 1009B. The content of Ta-riched MX precipitates increased with the increase of Ta content. The presence of them could pin the austenite grain boundaries and keep grains fine during solid solution at high temperature [36]. One possible explanation of the grain refinement from HEATs 1009A to 1009D could attribute to the enhanced pinning effect with the increase of Ta-riched MX precipitates content.

The solubility of tantalum in HEATs 1009A-D was calculated using the following solubility product equation of TaC in austenite and solution temperature [37] and the stoichiometric equation of TaC.

Solubility product equation:

$$\log[\mathrm{Ta}][\mathrm{C}] = 3.16 - \frac{7027}{T} \quad (1)$$

Stoichiometric equation:

$$\frac{\mathrm{Ta} - [\mathrm{Ta}]}{\mathrm{C} - [\mathrm{C}]} = \frac{180.95}{12} \quad (2)$$

where T is the solution temperature, [Ta] and [C] are the mass percent of solid solution of Ta and C, respectively. Table 3 shows the solubility of Ta and the precipitated TaC in HEATs 1009A-D at 1253 K and 1033 K. TaC_I is the undissolved TaC particle during the austenitizing process at 1253 K, and TaC_I is the precipitated particles during the tempered process at 1033 K.

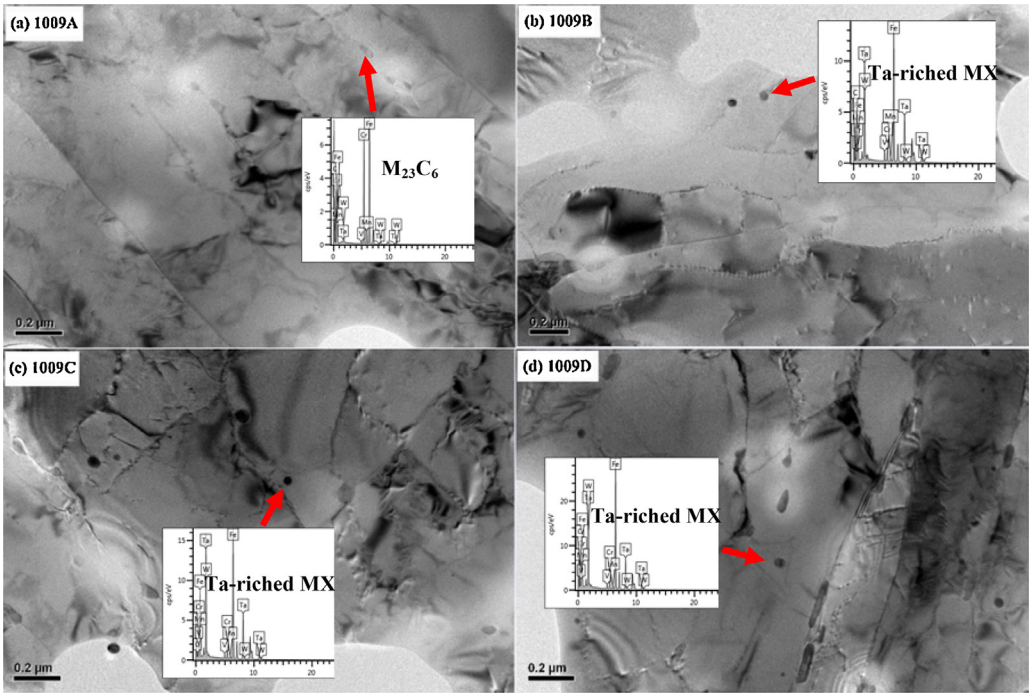

Fig. 3. TEM observation of the HEATs 1009A-D.

Table 3
The solubility and precipitation of tantalum in HEATs 1009A-D.

	T = 1253 K		T = 1033 K		
	[Ta]	TaC_I	[Ta]	TaC_I	TaC_I
1009A	0.11	0	0.0021	0	0.0266
1009B	0.0333	0.0477	0.0022	0.0477	0.0121
1009C	0.0385	0.1189	0.0025	0.1189	0.0384
1009D	0.0355	0.1541	0.0023	0.1541	0.0354

According to the numerical results, two kinds of TaC carbides are formed which can explain the microstructure observation results of two kinds of Ta-riched MX particles. TaC_I could be the coarse particle, while TaC_I is the fine particle. All of Ta is dissolved in HEAT 1009A at 1253 K, but there are TaC_I carbides in HEATs 1009B-D, the contents of which are 0.0477 wt%, 0.1189 wt% and 0.1541 wt%. It indicates that the coarse TaC particles gradually increase from HEATs 1009A to 1009D. Meanwhile, according to the results, the total TaC particles exhibit a same trend.

3.2. Tensile properties

Ultimate tensile strength (UTS) and yield strength (YS) results of tensile specimens are illustrated in Fig. 4. It shows that UTS and YS decrease firstly with Ta content increasing from 0.027 wt% to 0.15 wt%, then increase with Ta content increasing from 0.15 wt% to 0.18 wt% at RT, 573 K, 773 K and 873 K. Among the four HEATs, UTS and YS of HEATs 1009A and 1009D are higher than those of other HEATs at the same temperature, and UTS and YS of HEAT 1009A are the highest, while those of HEAT 1009C are the lowest. But there is little difference in strength with the change of Ta content. The differences in UTS and YS for HEATs 1009A and 1009C are 37.5 MPa and 62.5 MPa at RT, 25 MPa and 42.5 MPa at 573 K, 27.5 MPa and 32.5 MPa at 773 K, 25 MPa and 27.5 MPa at 873 K, respectively. The total elongation and reduction of area of tensile

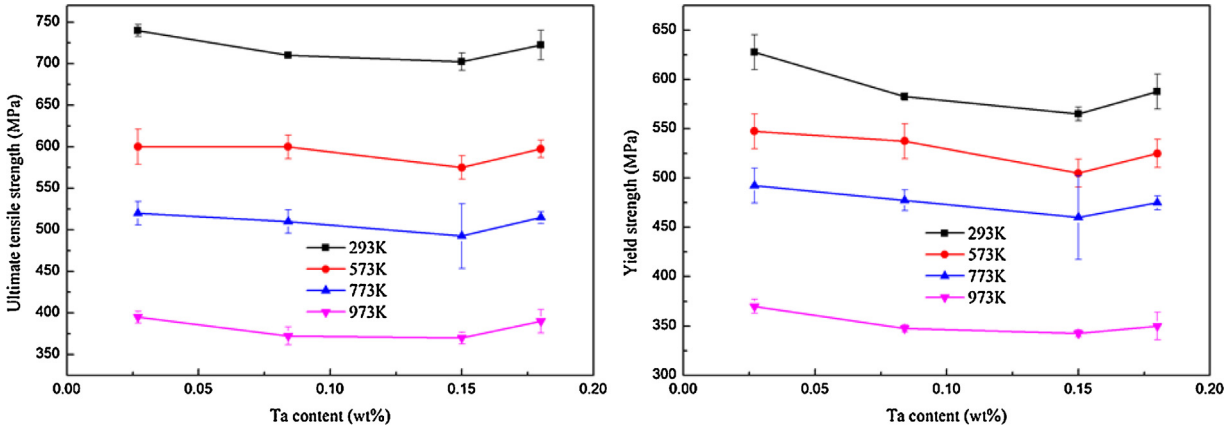

Fig. 4. Ultimate tensile strength and yield strength of HEATs 1009A-D.

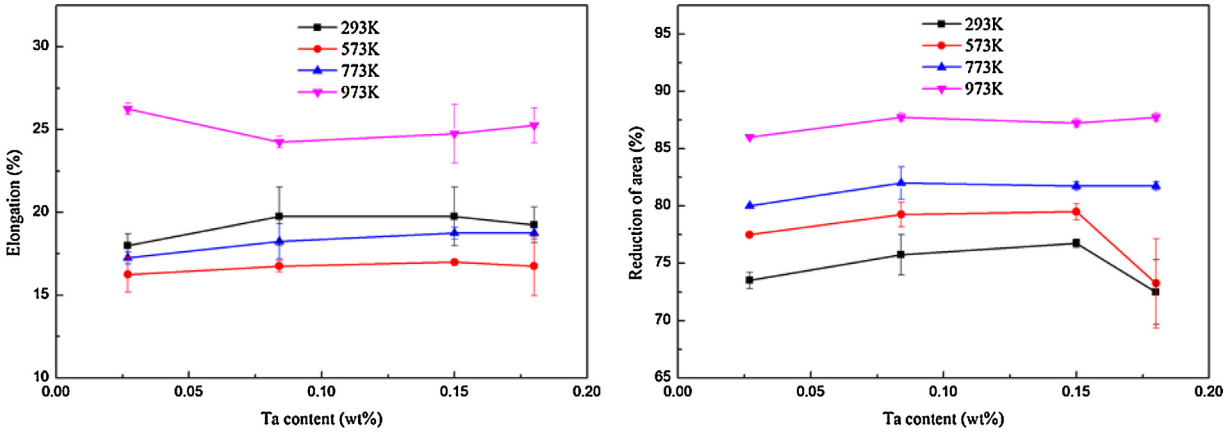

Fig. 5. Total elongation and reduction of area for HEATs 1009A-D.

specimens are shown in Fig. 5. All HEATs have similar total elongation and reduction of area. But the total elongation and reduction of area of HEATs 1009A and 1009D are lower than HEATs 1009B and 1009C at 293 K and 573 K, and the reduction of area has a sudden reduction for HEAT 1009D in particular.

The fracture appearance of the tensile specimens at RT and 873 K are shown in Figs. 6 and 7, respectively. There are dimples on the whole fracture surface, indicating that the fracture is ductile. At room temperature, compared with HEATs 1009B and 1009C, HEATs 1009A and 1009D have a part of larger size dimples as shown in Fig. 6. The non-uniformity of dimples size may be the possible explanation for their lower plasticity for HEATs 1009A and 1009D. As shown in Fig. 7, a large number of spherical precipitates can be observed in the dimples. The dimples are larger and deeper at 873 K than at RT, which indicates a better plasticity at higher temperature.

According to Hall–Petch's equation [38], the grain refinement is an effective method to improve the strength of metal. However, HEATs 1009C and 1009D with the finest grain have not demonstrated the highest strength as expected. It indicates that CLAM steel strengthening is the combination of multiple strengthening mechanisms. The strengthening of the alloy usually affected by different strengthening mechanisms such as fine-grain strengthening, solution strengthening, precipitation strengthening and dislocations strengthening [39,40]. As the solubility calculated above, Ta was saturated in the four HEATs, and other compositions were basically identical. So the solution strengthening of the four HEATs was basically consistent. Meanwhile, the four HEATs had basically same composition, identical machining and heat treatment conditions, and that was why dislocations strengthening was considered to be the same. Due to the presence of the precipitates, in addition to fine-grain strengthening, the precipitation strengthening was another

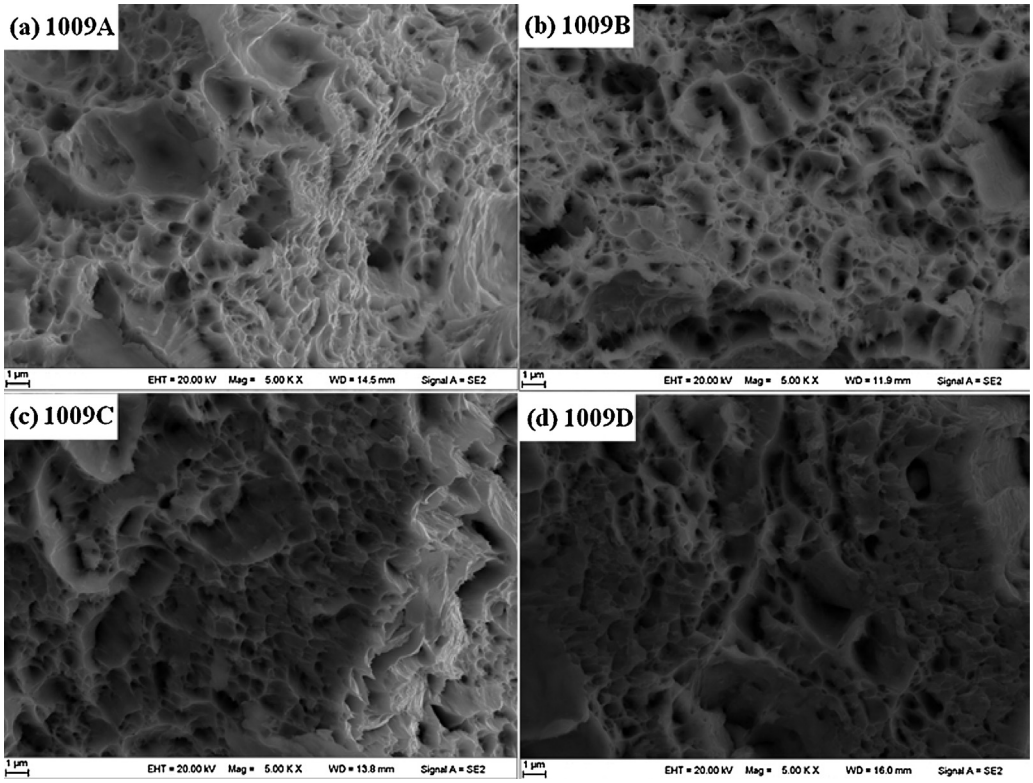

Fig. 6. SEM images of tensile fracture surfaces of HEATs 1009A-D at RT.

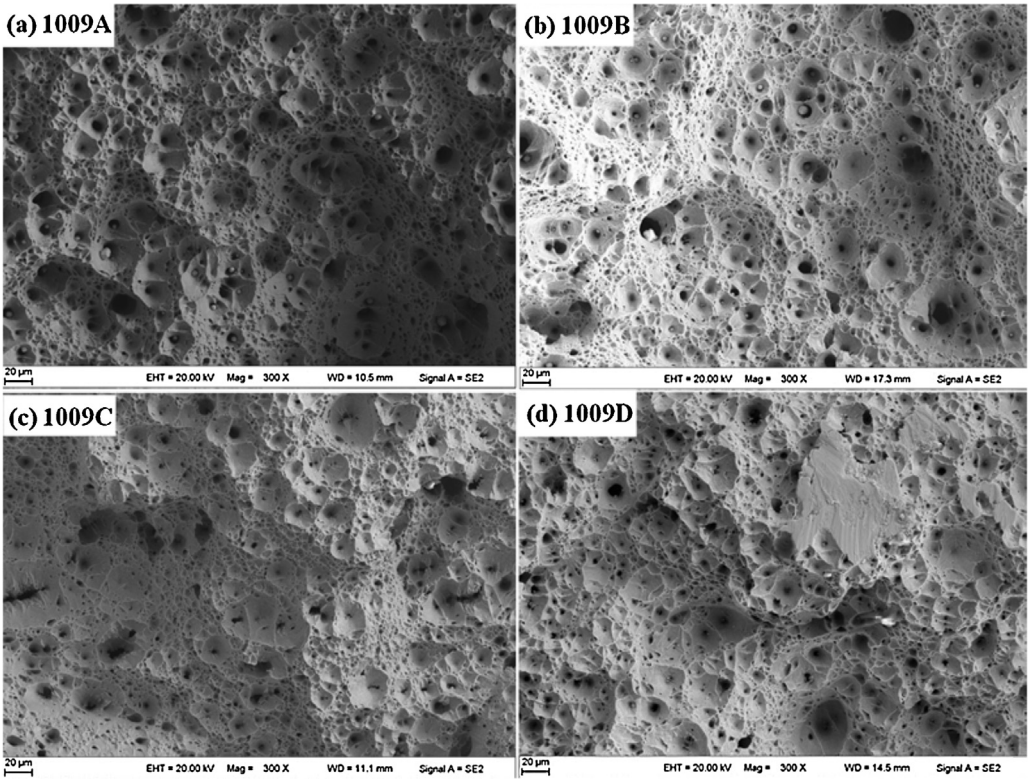

Fig. 7. SEM images of tensile fracture surfaces of HEATs 1009A-D at 873 K.

important factor for CLAM steel strengthening. The quantitative research on grain refinement had been carried out for years and the yield strength increment $\Delta\sigma_y$ of fine-grain strengthening can be expressed as the follow equation [13]:

$$\Delta\sigma_y = \Delta(k_b D^{-1/2}) \tag{3}$$

where k_b is a constant related to be interaction between grain boundaries and dislocations, D (m) is the average grain size. According to Ref. [13], the factor k_b of RAFM steel is 0.62 M $Nm^{-1.5}$ and D is the prior austenite grain diameter. The results show that $\Delta\sigma_y$ of HEATs 1009A-D are 126 MPa, 186 MPa, 215 MPa and 217 MPa, respectively, so the strength differences between HEAT 1009A and HEATs 1009B-D by fine-grain strengthening are 60 MPa, 89 MPa and 91 MPa, respectively. The experimental differences in YS between HEAT 1009A and HEATs 1009B-D are 45 MPa, 62.5 MPa and 40 MPa at RT. So the differences of precipitation strengthening of HEAT 1009A to that of HEATs 1009B-D are about −15 MPa, −26.5 MPa and −51 MPa, which indicates that the precipitation strengthening of HEAT 1009A is stronger than others. HEAT 1009A has the largest number of the Cr-riched $M_{23}C_6$ carbides, and the precipitation strengthening of Cr-riched $M_{23}C_6$ carbides is considered to be the main possible reason for HEAT 1009A which has the highest strength.

4. Conclusion

The effect of tantalum content on the microstructure and tensile properties of CLAM was investigated, the results of which are summarized as follows:

(1) The grain size decreases with the increase of Ta content. However, the effect of Ta content on the grain size refinement is no longer apparent under the condition of the conventional heat treatment when Ta content is raised.

(2) With the increase of Ta content, the content of Cr-riched $M_{23}C_6$ carbides decreases, and the size and the content of Ta-riched MX particles which was formed at 1253 K and 1033 K increase.

(3) The increase of Ta content of CLAM steel from 0.027 wt% to 0.18 wt% could affect the tensile properties by changing precipitates and grain size, but the effect of which is relatively small. The reason that HEAT 1009A has the highest UTS and YS may due to the precipitation strengthening of Cr-riched $M_{23}C_6$ carbides.

For the effect of Ta content on the tensile properties of CLAM steel, Ta content with 0.027 wt% is a better choice under the condition of the present study. This work is a part of the composition optimization research of CLAM steel and more investigations including impact, creep, fatigue and fracture toughness will be carried out to further optimize Ta content in the future.

Acknowledgements

This work was supported by the National Natural Science Foundation of China with Grant No. 51101148, the National Magnetic Confinement Fusion Science Program of China with Grant Nos. 2013GB108005 and 2014GB112003. The authors would like to thank Dr. Z. X. Xia and Mr. K. F. Li for their helps on this work and show great appreciation to other members in FDS Team for their support and contribution to this research.

References

[1] N. Baluc, D.S. Gelles, S. Jitsukawa, et al., Status of reduced activation ferritic/martensitic steel development, J. Nucl. Mater. 367–370 (2007) 33–41.
[2] R.J. Kurtz, A. Alamo, E. Lucon, et al., Recent progress toward development of reduced activation ferritic/martensitic steels for fusion structural applications, J. Nucl. Mater. 386–388 (2009) 411–417.
[3] Masato Akiba, Mikio Enoeda, Satoru Tanaka, Overview of the TBM R&D activities in Japan, Fusion Eng. Des. 85 (2010) 1766–1771.

[4] B. van der Schaaf, F. Tavassoli, C. Fazio, et al., The development of EUROFER reduced activation steel, Fusion Eng. Des. 69 (2003) 197–203.
[5] Q. Huang, C. Li, Y. Li, et al., Progress in development of China Low Activation Martensitic steel for fusion application, J. Nucl. Mater. 367–370 (2007) 142–146.
[6] R.L. Klueh, D.J. Alexander, M. Rieth, The effect of tantalum on the mechanical properties of a 9Cr–2W–0.25V–0.07Ta–0.1C steel, J. Nucl. Mater. 273 (1999) 146–154.
[7] H. Kayano, A. Kimura, M. Narui, et al., Effects of small changes in alloy composition on the mechanical properties of low activation 9%Cr-2%W steel, J. Nucl. Mater. 179–181 (1991) 671–674.
[8] Z.X. Xia, C. Zhang, N.Q. Fan, et al., Improve creep properties of reduced activation steels by controlling precipitation behaviors, Mater. Sci. Eng. A 545 (2012) 91–96.
[9] J. Vanaja, K. Laha, M.D. Mathew, et al., Effects of tungsten and tantalum on creep deformation and rupture properties of reduced activation ferritic-martensitic steel, Procedia Eng. 55 (2013) 271–276.
[10] H. Tanigawa, K. Shiba, T. Hirose, et al., 21st IAEA Fusion Energy Conference, Chengdu, China, October 16–22, 2006.
[11] Q. Huang, FDS Team, Development status of CLAM steel for fusion application, J. Nucl. Mater. 455 (2014) 649–654.
[12] Q. Huang, N. Baluc, Y. Dai, et al., Recent progress of R&D activities on reduced activation ferritic/martensitic steels, J. Nucl. Mater. 442 (2013) S2–S8.
[13] Y. Li, Q. Huang, Y. Wu, et al., Mechanical properties and microstructures of China low activation martensitic steel compared with JLF-1, J. Nucl. Mater. 367–370 (2007) 117–121.
[14] X. Chen, Y. Huang, B. Madigan, et al., An overview of the welding technologies of CLAM steels for fusion application, Fusion Eng. Des. 87 (2012) 1639–1646.
[15] Q.Y. Huang, Y.C. Wu, J.G. Li, et al., Status and strategy of fusion materials development in China, J. Nucl. Mater. 386–388 (2009) 400–404.
[16] Y. Wu, the FDS Team, Design analysis of the China dual-functional lithium lead (DFLL) test blanket module in ITER, Fusion Eng. Des. 82 (2007) 1893–1903.
[17] X. Chen, Q. Yuan, B. Madigan, et al., Long-term corrosion behavior of martensitic steel welds in staticmolten Pb–17Li alloy at 550 °C, Corros. Sci. 96 (2015) 178–185.
[18] Q. Huang, J. Li, Y. Chen, Study of irradiation effects in China low activation martensitic steel CLAM, J. Nucl. Mater. 329–333 (2004) 268–272.
[19] Y. Wu, FDS Team, CAD-based interface programs for fusion neutron transport simulation, Fusion Eng. Des. 84 (2009) 1987–1992.
[20] Y. Wu, J. Song, H. Zheng, et al., CAD-based Monte Carlo program for integrated simulation of nuclear system SuperMC, Ann. Nucl. Energy 82 (2015) 161–168.
[21] Y. Chen, Y. Wu, Conceptual study on high performance blanket in a spherical tokamak fusion-driven transmuter, Fusion Eng. Des. 49–50 (2000) 507–512.
[22] Y. Wu, Progress in fusion-driven hybrid system studies in China, Fusion Eng. Des. 63–64 (2002) 73–80.
[23] Y. Wu, L. Qiu, Y. Chen, Conceptual study on liquid metal center conductor post in spherical tokamak reactors, Fusion Eng. Des. 51–52 (2000) 395–399.
[24] Y. Wu, S. Zheng, X. Zhu, et al., Conceptual design of the fusion-driven subcritical system FDS-I, Fusion Eng. Des. 81 (2006) 1305–1311.
[25] Y. Wu, the FDS Team, Design status and development strategy of China liquid lithium-lead blankets and related material technology, J. Nucl. Mater. 367–370 (2007) 1410–1415.
[26] Y. Wu, FDS Team, Conceptual design activities of FDS series fusion power plants in China, Fusion Eng. Des. 81 (2006) 2713–2718.
[27] L. Qiu, Y. Wu, B. Xiao, et al., A low aspect ratio Tokamak transmutation system, Nucl. Fusion 40 (2000) 629–633.
[28] Y. Wu, J. Qian, J. Yu, The fusion-driven hybrid system and its material selection, J. Nucl. Mater. 307–311 (2002) 1629–1636.
[29] Y. Wu, J. Jiang, M. Wang, M. Jin, et al., A fusion-driven subcritical system concept based on viable technologies, Nucl. Fusion 51 (2011) 103036.
[30] Y. Wu, FDS Team, Conceptual design of the China fusion power plant FDS-II, Fusion Eng. Des. 83 (2008) 1683–1689.
[31] Y. Wu, FDS team, Fusion-based hydrogen production reactor and its material selection, J. Nucl. Mater. 386–388 (2009) 122–126.
[32] Y. Wu, FDS Team, Conceptual design and testing strategy of a dual functional lithium-lead test blanket module in ITER and EAST, Nucl. Fusion 47 (2007) 1533–1539.
[33] P. Fernández, A.M. Lancha, J. Lapeña, et al., Creep strength of reduced activation ferritic/martensitic steel Eurofer'97, Fusion Eng. Des. 75–79 (2005) 1003–1008.
[34] S. Liu, Q. Huang, L. Peng, et al., Microstructure and its influence on mechanical properties of CLAM steel, Fusion Eng. Des. 87 (2012) 1628–1632.
[35] Z.X. Xia, C. Zhang, Z.G. Yang, Control of precipitation behavior in reduced activation steels by intermediate heat treatment, Mater. Sci. Eng. A 528 (2011) 6764–6768.
[36] A. Alamo, J.C. Brachet, A. Castaing, et al., Physical metallurgy and mechanical behaviour of FeCrWTaV low activation martensitic steels: effects of chemical composition, J. Nucl. Mater. 258–263 (1998) 1228–1235.
[37] K. Narita, S. Koyama, Tetsu To Hagane 52 (1966) 788–791.
[38] N.J. Petch, J. Iron Steel Inst. 173 (1953) 25–28.
[39] Y.I. Hai-long, D.U. Lin-xiu, G.d. Wang, et al., Strengthening mechanism of a new 700 MPa hot rolled high strength steel, J. Iron Steel Res. 15 (2008) 76–80.
[40] V. Carretero Olalla, V. Bliznuk, N. Sanchez, et al., Analysis of the strengthening mechanisms in pipeline steels as a function of the hot rolling, Mater. Sci. Eng. A 604 (2014) 46–56.